

See discussions, stats, and author profiles for this publication at: <https://www.researchgate.net/publication/263942970>

A Family of Three-Dimensional Lanthanide-Zinc Heterometal-Organic Frameworks from 4,5-Imidazoledicarboxylate and Oxalate

ARTICLE in CRYSTAL GROWTH & DESIGN · APRIL 2011

Impact Factor: 4.89 · DOI: 10.1021/cg1015753

CITATIONS

67

READS

25

8 AUTHORS, INCLUDING:



Zhi-Gang Gu

Chinese Academy of Sciences

33 PUBLICATIONS 481 CITATIONS

[SEE PROFILE](#)



Weishan Li

South China Normal University

244 PUBLICATIONS 3,258 CITATIONS

[SEE PROFILE](#)

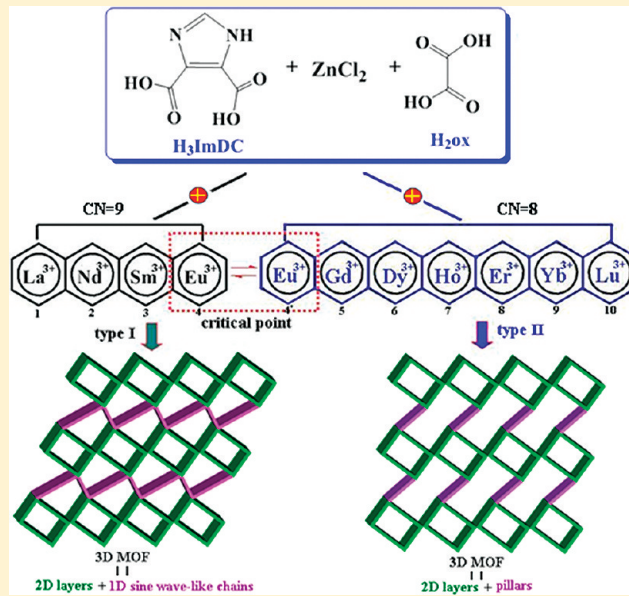
A Family of Three-Dimensional Lanthanide-Zinc Heterometal—Organic Frameworks from 4,5-Imidazoledicarboxylate and Oxalate and Oxalate

Zhi-Gang Gu, Hua-Cai Fang, Pei-Yi Yin, Long Tong, Yin Ying, She-Jun Hu, Wei-Shan Li, and Yue-Peng Cai*

School of Chemistry and Environment, Key Laboratory of Electrochemical Technology on Energy Storage and Power Generation of Guangdong Higher Education Institutes, Engineering Research Center of Materials and Technology for Electrochemical Energy Storage (Ministry of Education), South China Normal University, Guangzhou, 510006, China

Supporting Information

ABSTRACT: A family of lanthanide-zinc coordination polymers with two different types of three-dimensional (3-D) frameworks based on 4,5-imidazoledicarboxylic acid and oxalic acid, namely, $\{[\text{Ln}_2(\text{H}_2\text{O})_2\text{Zn}_4(\text{H}_2\text{O})_4(\text{ImDC})_4(\text{ox})]\cdot 6\text{H}_2\text{O}\}_n$ ($\text{Ln} = \text{La}$ (1), Nd (2), Sm (3), Eu (4), and $\text{H}_3\text{ImDC} = 4,5\text{-imidazoledicarboxylic acid}$, H_2ox = oxalic acid) and $\{[\text{Ln}_4(\text{H}_2\text{O})_4\text{Zn}_4(\text{H}_2\text{O})_4(\text{ImDC})_4(\text{ox})]\cdot 2\text{CH}_3\text{OH}\cdot 2\text{H}_2\text{O}\}_n$ ($\text{Ln} = \text{Eu}$ (4'), Gd (5), Dy (6), Ho (7), Er (8), Yb (9), and Lu (10)), were successfully constructed under certain conditions and characterized by elemental analysis, IR, thermogravimetric (TG), and single-crystal X-ray diffraction. The results reveal that compounds 1–4 (I structure) are isomorphous 3-D coordination frameworks containing two-dimensional (2-D) $[\text{Zn}_2(\text{ImDC})_2]$ layers and one-dimensional (1-D) $\text{Ln}_2(\mu_2\text{-O})_2(\text{ox})$ sine wave-like chains with 1-D square channels, while 4'–10 coordination polymers (II structure) are also isomorphous and feature 3-D pillar-layered coordination frameworks constructed from 2-D Zn -carboxylate $[\text{Zn}_2(\text{ImDC})_2]$ layers and $\text{Ln}_2(\text{ox})$ pillars with 1-D flat channels. The structural variation from I to II with the europium ion as a critical point, in which two types of europium complexes 4 and 4' can reversibly transform into each other, may be attributed to the lanthanide contraction effect. Meanwhile, the adsorption and photoluminescent properties of the partial compounds are also investigated.



INTRODUCTION

In recent years, the design and synthesis of 3d-4f heterometal—organic frameworks (HMOFs) are of great interest in view of not only their impressive structural diversity in architectures¹ but also by their versatile applications in the fields of chemical sensor, catalysis, gas storage and separation, fluorescence, magnetism, and so on.² It is well-known that the considerable change in the size of the Ln^{3+} ions from La^{3+} (1.06 Å) to Lu^{3+} (0.85 Å), which is often referred to as the lanthanide contraction, means that homologous compounds of lanthanides with appreciably different radii may differ in structure,³ so that the lanthanide contraction effect is now an important and effective route to construct diverse lanthanide compounds. Because 3d-4f heterometallic polymers can exhibit some special properties arising from the close proximity of dissimilar metal ions;⁴ however, their assembly is more complicated in comparison with homometallic ones. To date, there are a few reports on the assembly regularity

for infinite 3d-4f heterometallic compounds driven by the various Ln ions.^{1h}

Generally, the Ln ions prefer O- to N-donors, while d-block metal ions have a strong tendency to coordinate to both N- and O-donors. Thus, the ligands with N- and O-donors such as 4,5-imidazoledicarboxylic acid (ImDC^{3-}) serving as a bridge between Ln and TM ions, can elaborately be selected and employed to make heterometallic-organic frameworks. So far, H_3ImDC has been mainly used to make metal—organic frameworks (MOFs) with single transition metal (TM) or Ln ions,⁵ but the assembly in Ln -TM-organic frameworks remains relatively rare;⁶ in particular, the systematic investigation of Zn-4f heterometallic coordination polymers with luminescent and adsorption properties

Received: November 27, 2010

Revised: March 29, 2011

Published: April 19, 2011

remains less developed. Therefore, the introduction of group 12 metals of Zn into the Ln–organic frameworks not only should be a rational synthetic strategy but also could open the way to new luminescent and adsorbent materials.^{6b} At the same time, research on the coordination behavior of H₃ImDC-Zn-4f heterometallic complexes is one of the most essential elements of crystal engineering and coordination chemistry.

On the other hand, our research group has reported a series of 4f pyridine-2,6-dicarboxylate compounds with the diversity of Ln-based structures controlled by the radii of Ln ions, and the framework structures change from low to high dimension with a decrease in the Ln³⁺ radii.^{3c} In addition, based on ligand H₃Imdc, two high-dimensional lanthanide and two 3-D cadmium coordination frameworks with helical characters were also recently observed in our lab.⁷

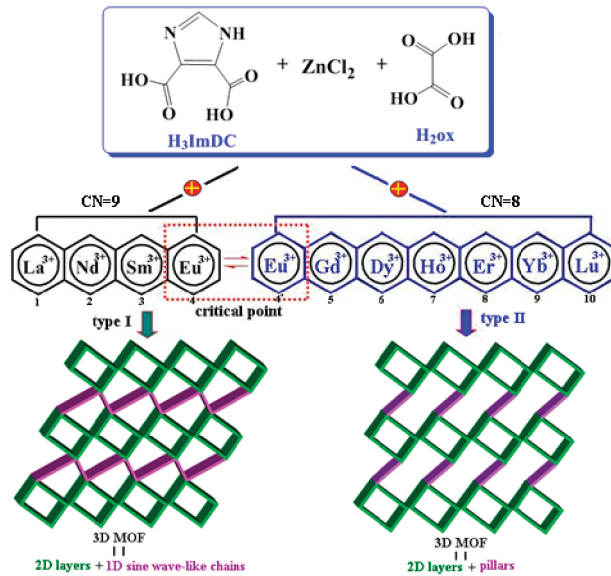
As part of our ongoing study of metal complexes of the dicarboxylic acid 4,5-imidazoledicarboxylic acid (ImDC³⁻), herein, we observed an intriguing example of the structural change for heterometallic 3d-4f-Imdc compounds driven by various lanthanide radii, in which the assembly rule is distinguished by all the known examples for the Ln compounds. The Ln³⁺-Zn²⁺-Imdc coordination polymers **1–10** were synthesized by means of self-assembly under similar conditions, in which they exhibit two different types of structures: {[Ln₂(H₂O)₂Zn₄(H₂O)₄(ImDC)₄-(ox)]·6H₂O}_n (Ln = La (**1**), Nd (**2**), Sm (**3**), and Eu (**4**), H₂ox = oxalic acid) for type I with monoclinic system and space group C₂/c; {[Ln₂(H₂O)₄Zn₄(H₂O)₄(ImDC)₄(C₂O₄)₂]·2CH₃OH·2H₂O}_n (Ln = Gd (**5**), Dy (**6**), Ho (**7**), Er (**8**), Yb (**9**), and Lu (**10**)) for type II with monoclinic system and space group P₂₁/c. As the Ln³⁺ radii decrease, their coordination numbers change from nine to eight with respective two blocks La³⁺ → Eu³⁺ (type I) and Eu³⁺ → Lu³⁺ (type II) with the europium ion as a critical point, in which two types of europium complexes **4** (type I) and **4'** (type II) can reversibly transform into each other. Obviously, the interesting example reported here may help us to further recognize the lanthanide contraction effect. To the best of our knowledge, this is the first example of systematically investigating the coordination chemistry and lanthanide contraction effect in the system of heterometallic Zn-4f as well as mixed dicarboxylate ligands ImDC³⁻ and ox²⁻.

■ EXPERIMENTAL SECTION

Physical Measurements. All materials were reagent grade obtained from commercial sources and used without further purification, and solvents were dried by standard procedures. Elemental analyses for C, H, N were performed on a Perkin-Elmer 240C analytical instrument. IR spectra were recorded on a Nicolet FT-IR-170SX spectrophotometer in KBr pellets. Thermogravimetric analyses were performed on Perkin-Elmer TGA7 analyzer with a heating rate of 10 °C/min in flowing air atmosphere. The luminescent spectra for the solid state were recorded at room temperature on Hitachi F-2500 and Edinburgh-FLS-920 with a xenon arc lamp as the light source. In the measurements of emission and excitation spectra the pass width is 5.0 nm. Nitrogen and hydrogen adsorption isotherms were taken on a Backman Coulter SA 3100 surface area and pore size analyzer.

Synthesis of the Compounds. For compounds **1–10**, 10 complexes were prepared by a similar procedure. A mixture of H₃ImDC (0.156 g, 1.0 mmol), Ln₂O₃ (0.25 mmol), ZnCl₂ (0.136 g, 1.0 mmol), oxalic acid (0.090 g, 1.0 mmol), methanol (5 mL), and deionized water (10 mL) was sealed in a 20 mL Teflon-lined stainless steel vessel and heated at 165 °C for 4 days, followed by cooling to 100 °C at a rate of

Scheme 1. Assembly of 11 Zn-Ln Compounds Tuned by Lanthanide Contraction Effect



10 °C/h, and held at this temperature for 10 h, then cooled to room temperature; finally the target products **1–10** were collected.

1. Yield 49% (based on the La). Elemental analysis calcd (%) for C₁₁H₁₄N₄O₁₆LaZn₂: C, 18.13; H, 1.92; N, 7.69. Found: C, 18.08; H, 1.90; N, 7.62. IR (KBr, cm⁻¹): 3453–3122(br), 1635(s), 1588(m), 1455(m), 1312(w), 1398(s), 1247(s), 1103(vs), 1005(w), 861(m), 821(m), 797(m), 662(s), 540(w).

2. Yield 58% (based on the Nd). Elemental analysis calcd (%) for C₁₁H₁₄N₄O₁₆NdZn₂: C, 18.12; H, 1.91; N, 7.68. Found: C, 18.09; H, 1.90; N, 7.62. IR (KBr, cm⁻¹): 3562–3121(br), 1633(s), 1590(m), 1453(m), 1337(w), 1395(s), 1244(m), 1116(vs), 858(m), 817(m), 789(m), 663(m).

3. Yield 52% (based on the Sm). Elemental analysis calcd (%) for C₁₁H₁₄N₄O₁₆SmZn₂: C, 18.11; H, 1.90; N, 7.67. Found: C, 18.05; H, 1.89; N, 7.63. IR (KBr, cm⁻¹): 3517–3222(br), 1636(s), 1456(m), 1315(w), 1399(s), 1248(s), 1100(vs), 1008(w), 865(m), 824(m), 794(m), 665(s), 549(w).

4. Yield 50% (based on the Eu). Elemental analysis calcd (%) for C₁₁H₁₄N₄O₁₆EuZn₂: C, 18.10; H, 1.89; N, 7.66. Found: C, 18.08; H, 1.88; N, 7.60. IR (KBr, cm⁻¹): 3496–3243(br), 1632(s), 1585(m), 1452(m), 1310(w), 1396(s), 1243(s), 1108(vs), 1005(w), 866(m), 823(m), 795(m), 660(s), 545(w).

5. Yield 61% (based on the Gd). Elemental analysis calcd (%) for C₂₃H₂₈N₈O₃₁Gd₂Zn₄: C, 18.54; H, 1.88; N, 7.52. Found: C, 18.51; H, 1.90; N, 7.50. IR (KBr, cm⁻¹): 3587–3333(br), 1672(s), 1560(m), 1459(s), 1401(m), 1299(s), 1270(w), 1247(s), 1103(vs), 972(m), 872(m), 845(w), 788(m), 744(s), 700(w), 665(s), 526(s), 462(m).

6. Yield 57% (based on the Dy). Elemental analysis calcd (%) for C₂₃H₂₈N₈O₃₁Dy₂Zn₄: C, 18.41; H, 1.87; N, 7.47. Found: C, 18.48; H, 1.86; N, 7.53. IR (KBr, cm⁻¹): 3598–3334(br), 1673(s), 1552(m), 1473(s), 1392(m), 1301(s), 1278(w), 1247(s), 1004(vs), 970(m), 869(m), 847(w), 790(m), 748(s), 698(w), 663(s), 518(s), 470(m).

7. Yield 48% (based on the Ho). Elemental analysis calcd (%) for C₂₃H₂₈N₈O₃₁Ho₂Zn₄: C, 18.35; H, 1.86; N, 7.45. Found: C, 18.39; H, 1.87; N, 7.41. IR (KBr, cm⁻¹): 3600–3336(br), 1677(s), 1557(m), 1474(s), 1399(m), 1304(s), 1276(w), 1245(s), 1100(vs), 968(m), 871(m), 844(w), 786(m), 745(s), 702(w), 664(s), 520(s), 466(m).

8. Yield 67% (based on the Er). Elemental analysis calcd (%) for C₂₃H₂₈N₈O₃₁Er₂Zn₄: C, 18.30; H, 1.86; N, 7.42. Found: C, 18.37; H,

1.84; N, 7.37. IR (KBr, cm^{-1}): 3592–3339(br), 1670(s), 1553(m), 1478(s), 1393(m), 1306(s), 1273(w), 1242(s), 1107(vs), 963(m), 877(m), 847(w), 782(m), 744(s), 707(w), 667(s), 522(s), 463(m).

9. Yield 63% (based on the Yb). Elemental analysis calcd (%) for $\text{C}_{23}\text{H}_{28}\text{N}_8\text{O}_{31}\text{Yb}_2\text{Zn}_4$: C, 18.16; H, 1.84; N, 7.37. Found: C, 18.25; H, 1.85; N, 7.31. IR (KBr, cm^{-1}): 3586–3334(br), 1675(s), 1552(m), 1472(s), 1391(m), 1300(s), 1271(w), 1242(s), 1104(vs), 962(m), 873(m), 846(w), 786(m), 742(s), 667(s), 524(s), 462(m).

10. Yield 65% (based on the Lu). Elemental analysis calcd (%) for $\text{C}_{23}\text{H}_{28}\text{N}_8\text{O}_{31}\text{Lu}_2\text{Zn}_4$: C, 17.88; H, 1.81; N, 7.25. Found: C, 17.95; H, 1.87; N, 7.22. IR (KBr, cm^{-1}): 3581–3332(br), 1679(s), 1587(m), 1454(s), 1393(m), 1298(s), 1272(w), 1249(s), 1102(vs), 959(m), 878(m), 779(m), 743(s), 664(s), 597(m), 459(m).

Reversible Conversions Between 4 and 4'. The compound 4' can be transformed by a single crystal or bulk crystals of the corresponding compounds 4 (10^{-5} mol) at 40–55 °C for 5 h under the atmosphere of methanol. Reversibly, compound 4 can be also obtained by placing a single crystal or bulky crystals of 4' in the atmosphere of water at about 50 °C for 3 h. And bulky crystals of 4 and 4' for single-crystal X-ray diffraction and other measurements, respectively.

X-ray Data Collection and Structure Refinement. Data collections were performed at 298 K on a Bruker Smart Apex II diffractometer with graphite-monochromated Mo K α radiation ($\lambda = 0.71073 \text{ \AA}$) for 11 compounds **1–4**, **4'**, and **5–10**. Absorption corrections were applied by using the multiscan program SADABS.⁸ Structural solutions and full-matrix least-squares refinements based on F^2 were performed with the SHELXS-97⁹ and SHELXL-97¹⁰ program packages, respectively. All the non-hydrogen atoms were refined anisotropically. The hydrogen atoms on organic motives were placed at calculated position, and the coordinated water hydrogen atoms were located from difference maps and refined with isotropic temperature factors. All hydrogen atoms of the uncoordinated solvent water molecules have not been added. Details of the crystal parameters, data collections, and refinements for complexes **1–4**, **4'**, and **5–10** are summarized in Table 1. Selected bond lengths and angles are shown in Table S1. Further details are provided in Supporting Information. CCDC 801559, 801560, 801561, 801562, 801563, 801564, 801565, 801566, 801567, 801568 and 801569 are for 11 new compounds **1–4**, **4'**, and **5–10**, respectively.

RESULTS AND DISCUSSION

Synthesis and General Characterization of Compounds 1–10.

We tried to obtain these single crystals from a conventional solution method using the reactions of oxalic acid with a mixture of ZnCl_2 , 4,5-imidazoledicarboxylic acid, and lanthanide oxides. Unfortunately, only uncharacterized white viscous precipitates were obtained. Solvothermal synthesis has been proven to be a powerful method for the construction of organic–inorganic hybrid materials because at higher temperature the reaction becomes faster, thus leading to a higher degree of reversibility in the process of crystal growth. As expected, high-quality single crystals of **1–10** were obtained when the reactions of Ln_2O_3 with a mixture of ZnCl_2 , 4,5-imidazoledicarboxylic acid, and oxalic acid in water containing a little methanol were carried out at 165 °C for 4 days under solvothermal conditions. Although the reaction conditions are similar, compounds **1–4** with space group $C2/c$ differ from compounds **5–10** with space group $P2_1/c$. Interestingly, compound **4** may be converted to **4'** in the atmosphere of methanol at 50 °C for 5 h; conversely, complex **4'** can be also reversibly transformed into the complex **4** in the atmosphere of water for 3 h. Unfortunately, we did not directly obtain compound **4'** through the synthetic strategy

similar to those of complexes **1–10** though many attempts were made.

The structures of the complexes were identified by satisfactory elemental analysis, IR, and X-ray diffraction. The IR spectra of **1–10** are similar. The strong and broad absorption bands in the range of 3100–3600 cm^{-1} in compounds may be assigned to the characteristic peaks of $\nu_{\text{O}-\text{H}}$ stretching vibrations from water molecules. The strong vibrations appearing around 1635, 1590, and 1450 cm^{-1} correspond to the asymmetric and symmetric stretching vibrations of the carboxyl group, respectively.¹¹ The absence of strong bands ranging from 1690 to 1730 cm^{-1} indicates that the ligands are deprotonated.

Because complexes **1–4** (**I**), and **4', 5–10** (**II**) are isomorphous, respectively, compounds **3** and **6** were selected as two representatives to examine their thermal stability. The thermogravimetric analysis (TGA) curve of compound **3** reveals only one step of weight loss. The change started at 164 °C, corresponding to the release of three solvent water molecules and three coordinated water molecules. The observed weight loss of 14.6% is very consistent with the calculated value (14.7%). The second weight loss above 410 °C corresponds to the decomposition of the coordination network. The TGA curve of compound **6** also shows that the continuous weight losses in the temperature range of 100–180 °C are due to the removal of one solvate water molecule, one free methanol molecule, and four coordinated water molecules. The observed weight loss of 16.2% is in good agreement with the calculated value (16.3%). When the temperature reached 350 °C, the MOF was decomposed. In this system, **I** is more thermostable than **II** from the experimental data.

Description of Crystal Structures of Type I Complexes. $\{[\text{Ln}_2(\text{H}_2\text{O})_2\text{Zn}_4(\text{H}_2\text{O})_4(\text{ImDC})_4(\text{ox})]\cdot6\text{H}_2\text{O}\}_n$ ($\text{Ln} = \text{La}$ (**1**), Sm (**2**), Nd (**3**), and Eu (**4**)). Four compounds of **I** are isostructural, and thus only the structure of complex **3** is described in detail. The structure of **3** features a 3-D Sm(III)–Zn(II) heterometallic organic framework which is made up of 2-D $[\text{Zn}_2(\text{ImDC})_2]$ layers connected by 1-D $\text{Ln}_2(\mu_2\text{O})_2(\text{ox})$ sine wave-like chains with 1-D square channels. Figure 1 shows the coordination environment of Zn(II) and Sm(III) ions in **3**. The coordination environment around the Zn1 ion, located in hexa-coordinated octahedron geometry, is coordinated by three nitrogen atoms and three oxygen atoms from three ImDC³⁻ ligands, while the Zn2 ion is five-coordinated with trigonal bipyramidal geometry surrounded by one nitrogen and two oxygen atoms which derived from two crystallographic independent ImDC³⁻ ligands, and two coordinated water molecules. The Zn–O distances are in the range of 1.986(3)–2.301(3) Å and the Zn–N distances from 2.019(4) to 2.092(4) Å, which are in agreement with those observed for the penta-/hexa-coordinated Zn atom in carboxylate complexes.¹² In **3**, the central Sm(III) atom is nine-coordinated in a distorted tricapped trigonal prismatic geometry with six oxygen atoms from three ImDC³⁻ ligands, two O atoms from one oxalate ligand, and one O atom from the coordinated water molecule, respectively. The Sm–O bond distances range from 2.378(3) to 2.813(3) Å. The bond angles of O–Sm–O are in the range of 47.67(9)–153.33(9)° comparable to those in other Ln carboxylate complexes observed in our previous papers.^{3c,12d} In this structure, the ImDC³⁻ ligand exhibits two kinds of different coordination modes **A** and **B** as depicted in Scheme 2. In the coordination mode **A**: the nitrogen atom coordinates to the zinc center and the 4,5-carboxylate oxygen atoms chelate/bridge the Sm(III) and Zn(II) centers with the

Table 1. Crystal Data and Structure Refinement of 11 Compounds 1–4, 4', and 5–10

	1	2	3	4	4'	5
chemical formula	C ₁₁ H ₁₄ N ₄ O ₁₆ LaZn ₂	C ₁₁ H ₁₄ N ₄ O ₁₆ NdZn ₂	C ₁₁ H ₁₄ N ₄ O ₁₆ SmZn ₂	C ₁₁ H ₁₄ N ₄ O ₁₆ EuZn ₂	C ₂₃ H ₂₈ N ₈ O ₃₁ Eu ₂ Zn ₄	C ₂₃ H ₂₈ N ₈ O ₃₁ Gd ₂ Zn ₄
M	727.91	733.24	739.35	740.96	1477.93	1488.51
crystal system	monoclinic	monoclinic	monoclinic	monoclinic	monoclinic	monoclinic
space group	C2/c	C2/c	C2/c	C2/c	P2(1)/c	P2(1)/c
a / Å	24.482(3)	24.5039(13)	24.5105(14)	24.5105(14)	10.5125(9)	10.4826(6)
b / Å	9.8078(13)	9.8214(5)	9.8438(6)	9.8438(6)	10.1534(9)	10.1291(6)
c / Å	19.763(4)	19.6019(17)	19.4721(18)	19.4721(18)	19.7706(18)	19.7566(12)
α / °	90	90	90	90	90	90
β / °	125.7210(10)	126.0280(10)	126.1580(10)	126.1580(10)	103.2370(10)	103.1590(10)
γ / °	90	90	90	90	90	90
V/Å ³	3852.6(11)	3815.1(4)	3793.3(5)	3793.3(5)	2054.2(3)	2042.7(2)
Z	8	8	8	8	2	2
T/K	298 (2)	298(2)	298(2)	298(2)	298(2)	298(2)
F(000)	2824	2848	2864	2872	1432	1436
D _{calcd} /g cm ⁻³	2.510	2.553	2.589	2.595	2.389	2.420
μ / mm ⁻¹	4.746	5.274	5.663	5.874	5.422	5.629
λ / Å	0.71073	0.71073	0.71073	0.71073	0.71073	0.71073
R _{int}	0.0434	0.0260	0.0200	0.0202	0.0254	0.0261
data/restraint/parm	3391/9/302	3357/10/302	3341/9/302	3429/9/326	3609/31/342	3591/31/342
GOF	1.089	1.006	1.069	1.076	1.018	1.066
R ₁ [I = 2σ(I)] ^a	0.0377	0.0245	0.0242	0.0238	0.0262	0.0239
wR ₂ [I = 2σ(I)] ^b	0.0715	0.0557	0.0564	0.0576	0.0662	0.0611
	6	7	8	9	10	
chemical formula	C ₂₃ H ₂₈ N ₈ O ₃₁ Dy ₂ Zn ₄	C ₂₃ H ₂₈ N ₈ O ₃₁ Ho ₂ Zn ₄	C ₂₃ H ₂₈ N ₈ O ₃₁ Er ₂ Zn ₄	C ₂₃ H ₂₈ N ₈ O ₃₁ Yb ₂ Zn ₄	C ₂₃ H ₂₈ N ₈ O ₃₁ Lu ₂ Zn ₄	
M	1499.01	1503.87	1508.53	1520.09	1543.99	
crystal system	monoclinic	monoclinic	monoclinic	monoclinic	monoclinic	
space group	P2(1)/c	P2(1)/c	P2(1)/c	P2(1)/c	P2(1)/c	
a / Å	10.3993(7)	10.4586(12)	10.3886(12)	10.4186(9)	10.3486(12)	
b / Å	10.2250(7)	10.2348(12)	10.2148(12)	10.2243(10)	10.1148(12)	
c / Å	19.7676(13)	19.738(2)	19.798(2)	19.5891(7)	19.398(2)	
α / °	90	90	90	90	90	
β / °	103.8140(10)	103.558(2)	103.558(2)	103.602(2)	102.258(2)	
γ / °	90	90	90	90	90	
V/Å ³	2041.1(2)	2055.6(4)	2042.4(4)	2028.2(3)	1984.2(4)	
Z	2	2	2	2	2	
T/K	298 (2)	298(2)	298(2)	298(2)	298(2)	
F(000)	1444	1448	1452	1460	1488	
D _{calcd} /g cm ⁻³	2.439	2.430	2.453	2.489	2.584	
μ / mm ⁻¹	6.044	6.216	6.491	7.010	7.431	
λ / Å	0.71073	0.71073	0.71073	0.71073	0.71073	
R _{int}	0.0248	0.0251	0.0294	0.0431	0.0412	
data/restraint/parm	3574/31/342	3625/31/342	3592/31/342	3572/31/342	3476/31/342	
GOF	0.940	1.040	1.065	1.020	1.028	
R ₁ [I = 2σ(I)] ^a	0.0241	0.0227	0.0271	0.0315	0.0315	
wR ₂ [I = 2σ(I)] ^b	0.0592	0.0540	0.0671	0.0637	0.0680	

^a R₁ = Σ||F_o| - |F_c||/|F_o|. ^b wR₂ = [Σw(F_o² - F_c²)²/Σw(F_o²)²]^{1/2}, where w = 1/[σ²(F_o²) + (aP)₂ + bP]. P = (F_o² + 2F_c²)/3.

$\mu_5\text{-}\eta^1\text{:}\eta^2\text{:}\eta^2\text{:}\eta^1\text{:}\eta^1$ -bridging mode. In coordination mode B: the nitrogen atom coordinates to the zinc center, while the 4,5-carboxylate oxygen atoms also coordinate to samarium and zinc centers with the $\mu_3\text{-}\eta^1\text{:}\eta^1\text{:}\eta^1\text{:}\eta^1\text{:}\eta^1$ -bridging mode. The carboxyl groups of organic ligands are fully deprotonated, in agreement with the IR analysis. On the basis of the two

coordination modes of ligand ImDC³⁻, each 10 Zn(II) atoms and eight ImDC³⁻ ligands are connected each other to give a parallelogram building block unit with chair-conformation (Figure 2a), and then through offset parallel packing, these units are extended into a 3-connected 2-D [Zn(ImDC)]₂ layer with 6³ topology along the b axis as shown in Figure 2b.

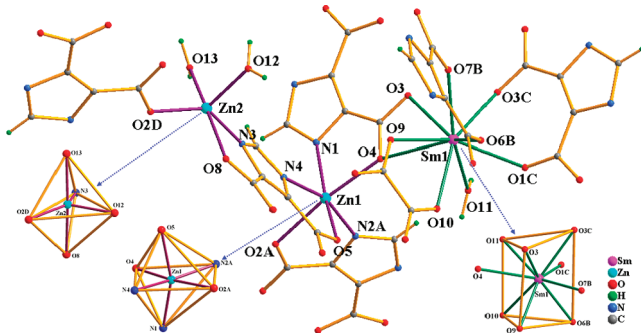


Figure 1. The coordination environments of the Zn^{II} ion and Sm^{III} ion in compound 3. Symmetry codes: (A) $1.5 - x, 0.5 + y, 0.5 - z$; (B) $2 - x, y, 0.5 - z$; (C) $2 - x, 1 - y, 1 - z$; (D) $x, -y, -0.5 + z$.

Scheme 2. Three Coordination Modes of ImDC^{3-} Ion in 6

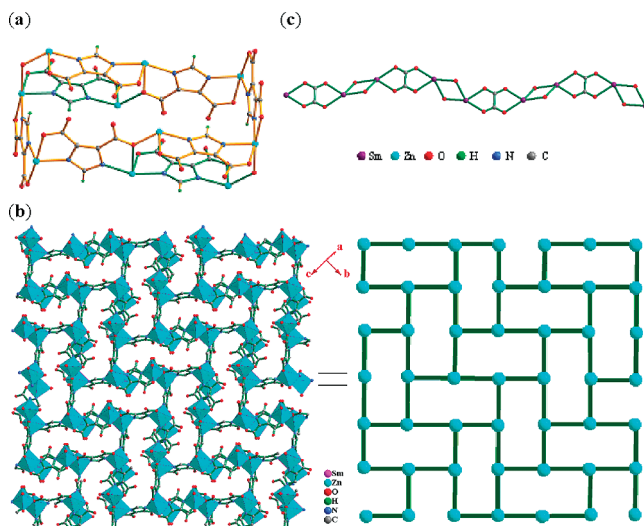
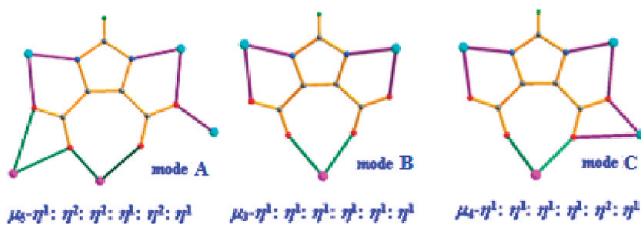


Figure 2. In 3, (a) building block unit $[\text{Zn}_{10}(\text{ImDC})_8]$ with chair conformation. (b) 3-connected Zn-containing layer with 6^3 topology. (c) 1-D infinite $[\text{Ln}_2(\mu_2\text{-O})_2(\mu_2\text{-ox})]_n$ sine wave-like chain along the c axis.

On the other hand, the oxalate dianion behaves as the $\mu_2\text{-}\kappa^4\text{O}$ bridges, connecting the adjacent two $\text{Sm}(\text{III})$ ions combined with the bridging effect of $\mu^2\text{-O}_3$ from ImDC^{3-} into a 1-D infinite $[\text{Ln}_2(\mu_2\text{-O})_2(\mu_2\text{-ox})]_n$ sine wave-like chain and the distances between $\text{Sm}(\text{III})$ ions are $4.146(7)$ and $6.308(8)$ Å (Figure 2c). Furthermore, 1D Ln-containing chains and 2D Zn-containing layers are further extended by $\text{Sm}-\text{O}$ coordination bonds to result in a 3-D chain-layer MOF with the 1-D square channels accommodated by the coordinated and uncoordinated water molecules with about 7.3×6.0 Å size along the

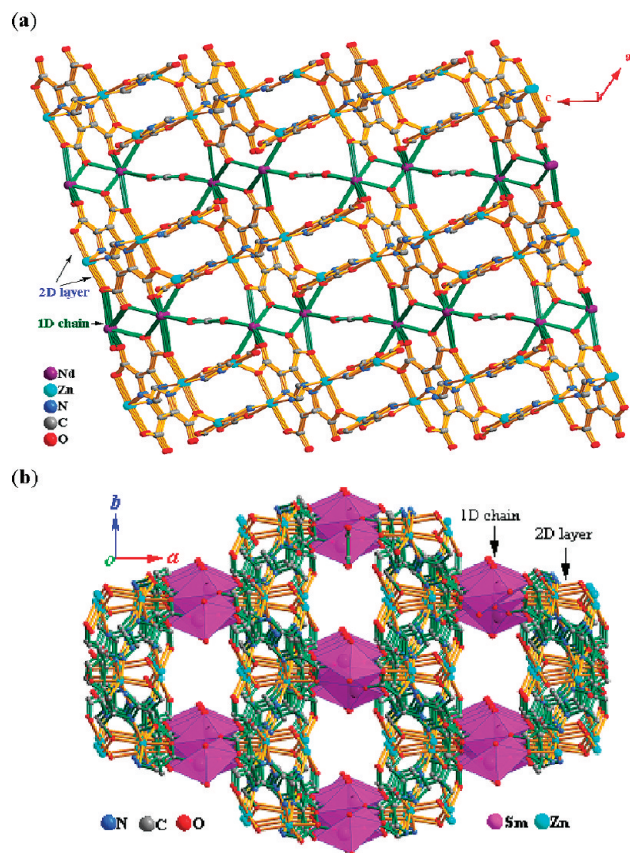


Figure 3. 3-D chain-layer MOF with the 1-D square channels (a) along the b axis, (b) along the c axis. The coordinated and lattice water molecules as well as hydrogen atoms are omitted for clarity.

c axis, and the distance between adjacent layers is about 7.32 Å (Figure 3).

Type II Structure of $\{[\text{Ln}_2(\text{H}_2\text{O})_4\text{Zn}_4(\text{H}_2\text{O})_4(\text{ImDC})_4(\text{C}_2\text{O}_4)\}_2\text{CH}_3\text{OH}\cdot 2\text{H}_2\text{O}\}_n$ ($\text{Ln} = \text{Gd}$ (5), Dy (6), Ho (7), Er (8), Yb (9), and Lu (10)). The reaction of H_3ImDC and H_2Ox with Ln_2O_3 and ZnCl_2 under the same hydrothermal condition generates six 3-D coordination polymers 5–10 with II structure. Here compound 6 was selected to represent the structures of II. The X-ray structural analysis of 6 reveals that it is a 3-D $\text{Dy}(\text{III})-\text{Zn}(\text{II})$ heterometallic organic framework which consists of 2-D $[\text{Zn}(\text{ImDC})_2]$ layers and $[\text{Ln}_2(\text{ox})]$ pillars with 1-D flat channels. Its asymmetrical unit is composed of two zinc ions, one dysprosium ion, two independent ImDC^{3-} ligands, one-half oxalate ligand which lies about an inversion center, four coordinated water molecules, and one lattice methanol molecule and one lattice water molecule.

Compared with compound 3, both $\text{Zn}(\text{II})$ atoms in 6 have the distorted octahedral coordination geometry. $\text{Zn}1$ atom coordinates to three ImDC^{3-} anions by using three oxygen atoms and three nitrogen atoms from three different ImDC^{3-} anions and $\text{Zn}2$ atom coordinates to two ImDC^{3-} anions by using three oxygen atoms and one nitrogen atom and two coordinated water molecules as shown in Figure 4.

The $\text{Zn}1-\text{O}$ bond distances are in the range of $2.171(2)-2.507(2)$ Å which are shorter than that of $\text{Zn}2-\text{O}$ [$2.024(2)-2.752(2)$ Å considering weak interaction of $\text{Zn}2\cdots\text{O}_3$ (2.852 Å)]. The $\text{Zn}-\text{N}$ bond distances are in the range of $1.995(2)-2.073(2)$ Å (Table S1, Supporting Information). The

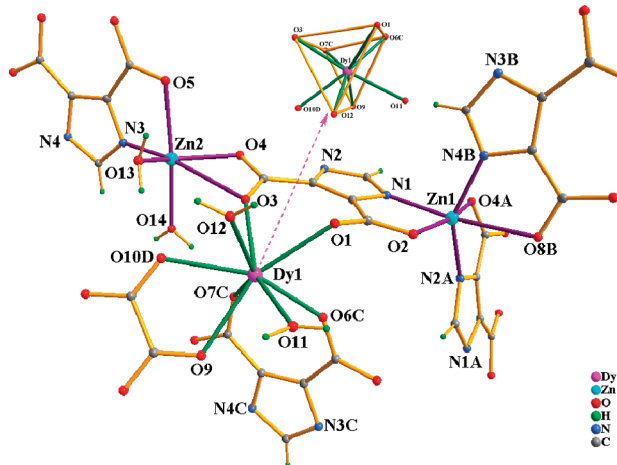


Figure 4. The coordination environments of the Zn^{II} ion and Sm^{III} ion in **6**. Symmetry codes: (A) $1 - x, 0.5 + y, 0.5 - z$; (B) $x, 0.5 - y, 0.5 + z$; (C) $x, 1 + y, z$; (D) $2 - x, 1 - y, -z$.

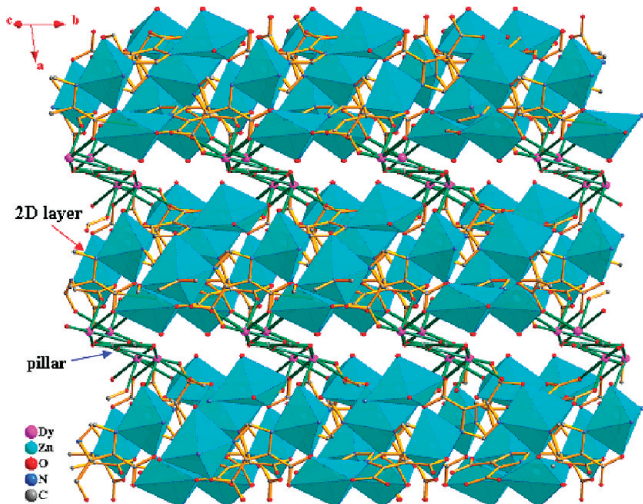


Figure 5. 3-D pillar-layer MOF with the 1-D flat channels along the *c* axis. The coordinated and lattice water molecules, uncoordinated methanol molecule as well as hydrogen atoms are omitted for clarity.

Dy(III) atom is eight-coordinated in a bicapped trigonal prismatic coordination geometry by four oxygen atoms from two ImDC²⁻ ligands, two oxygen atoms from the oxalate anions, and two oxygen atoms from two coordinated water molecules, respectively. The Dy–O bond distances range from 2.299(2) to 2.475(2) Å. The bond angles of O–Dy–O are in the range of 65.82(5) to 152.09(5)° (Table S1, Supporting Information). Similarly, the ImDC³⁻ ligand in **6** also adopts two kinds of different coordination modes with mode B and C as depicted in Scheme 2, in which mode C: $\mu_3\text{-}\eta^1\text{:}\eta^1\text{:}\eta^1\text{:}\eta^1\text{:}\eta^2\text{:}\eta^1$ is different from mode A of compound **3**. On the basis of two coordination modes of ImDC³⁻ ligand, the building block unit consisting of 10 Zn(II) atoms and eight ImDC³⁻ ligands with *chair*-conformation and 2-D zinc-containing layers also exist in compound **6** similar to **3** (Figures S2–3, Supporting Information). However, a 3-D heterometallic organic framework further extended with 1-D flat channels (ca. 7.9×4.5 Å size) in compound **6** is a $[\text{Zn}(\text{ImDC})_2]$ layers- $[\text{Ln}_2(\text{ox})]$ pillars structure rather than a chain-layer one as that in **3** (Figures 5 and S4, Supporting Information).

Structural Change and Reversible Transformation. As all the complexes **1**–**10** were synthesized using a similar procedure, two types of different crystal structures obtained provide a fair assessment of the critical influence of lanthanide contraction in the 3d-4f heterometallic system. La³⁺-Eu³⁺ have the larger ionic radius among all lanthanides, which makes La³⁺-Eu³⁺ possible to possess up to nine coordination sites. In order to satisfy the nine-coordinated potential, the ImDC³⁻ anion adopts two coordination modes A and B (Scheme 2). In mode A, two carboxyl groups via $\mu_2\text{-}\eta^1\text{:}\eta^2\text{:}\eta^1$ manner bridge two Dy³⁺ ions, resulting in the formation of a 1-D sine wave-like chain $[\text{Ln}_2(\mu_2\text{-O})_2(\text{ox})]_n$ (Figure 2c), which is further extended into a final 3-D chain-layer network (**I**). In contrast, the heavier lanthanide ions Sm³⁺-Lu³⁺ have the smaller ionic radius and eight-coordinated sites higher stability. In this case, chelating connections of the carboxyl groups of ImDC³⁻ are no longer necessary, and two carboxyl groups in complexes **5**–**10** are only both $\mu\text{-}\eta^1\text{:}\eta^1$ bridge-connecting to one Ln³⁺ ion to form two coordination modes B and C of ImDC³⁻ (Scheme 2), based on which 2-D $[\text{Zn}(\text{ImDC})_2]$ layer and $[\text{Ln}_2(\text{ox})]$ pillar construct the final 3-D pillar-layer network (**II**).

From the above results, it is noted that various coordination modes of the carboxyl groups of ImDC³⁻, caused by the lanthanide contraction, give rise to the different structures of the Ln-Zn-ImDC complexes though they are in the 3d-4f heterometallic system. In other words, the structural change of the Ln-Zn-ImDC complexes are still controlled by lanthanide contraction (Scheme 1) similar to homologous compounds of lanthanides. Moreover, we have also compared the average Ln–O bond lengths among the Ln-Zn-ImDC complexes (Table S1, Supporting Information). The average lengths between the lanthanide and O atoms are decreasing continuously from 2.553 (**1**), 2.512 (**2**), 2.490 (**3**), 2.487 (**4**), 2.426 (**4'**), 2.410 (**5**), 2.389 (**6**), 2.383 (**7**), 2.376 (**8**), 2.346 (**9**) to 2.323 Å (**10**).

Conversion between structural types **I** and **II** have been tried, and the results show that only compound **4** (**I**) may be reversibly converted into compound **4'** (**II**) under appropriate conditions. At about 50 °C or so, under the atmosphere of methanol/water, **4** and **4'** may be reversibly transformed into each other (Figure S5, Supporting Information); however, for other lanthanide Ln-Zn-ImDC complexes in the system, the conversion cannot be carried out under the same conditions. Obviously, in the present case, europium ion may serve as a critical point in the structural variation from **I** to **II**.

Luminescent and Adsorption Properties. The luminescent behaviors of compounds **3** (Sm), **4** (Eu), and **6** (Dy) were investigated in the solid state at room temperature. The emission spectrum of compound **3** at $\lambda_{\text{ex}} = 398$ nm is shown in Figure S6a, in which four peaks at 560, 594, 640, and 699 nm are assigned to the ${}^4G_{5/2} \rightarrow {}^6H_{5/2}$, ${}^4G_{5/2} \rightarrow {}^6H_{7/2}$, ${}^4G_{5/2} \rightarrow {}^6H_{9/2}$, and ${}^4G_{5/2} \rightarrow {}^6H_{11/2}$ transitions of the Sm(III) ion. The ${}^4G_{5/2}$ emission lifetime (21 μ s) of the Sm³⁺ compound **3** is shorter than those reported for most complexes of Sm³⁺ with β -diketonate ligands¹³ but is comparable with those observed for complexes of Sm³⁺ with iminodiacetic acid.¹⁴

From Figure S6b, the emission spectrum of the complex **4** was obtained when excited at 395 nm, and its emission peaks show moderately strong bands at 579, 593, 620 nm and two weak bands peaked at 651 and 702 nm, corresponding to the electronic transition of ${}^5D_0 \rightarrow {}^7F_0$, ${}^5D_0 \rightarrow {}^7F_1$, ${}^5D_0 \rightarrow {}^7F_2$, and ${}^5D_0 \rightarrow {}^7F_3$, ${}^5D_0 \rightarrow {}^7F_4$, respectively. The symmetry-forbidden weak emission peak ${}^5D_0 \rightarrow {}^7F_0$ at 580 nm indicates that the Eu(III) ions are

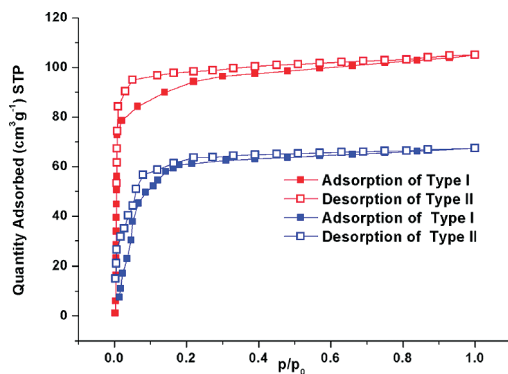


Figure 6. Isotherms of adsorption and desorption of nitrogen for 3 (red) and 6 (blue) at 77 K.

located on a low symmetry site. The emission peak $^5D_0 \rightarrow ^7F_1$ at 593 nm is a magnetic dipole transition, and its intensity is almost independent upon the crystal field change acting on the Eu(III) ions. The most intense emission band at 620 nm suggests that it is an electric dipole transition and that the ligand is suitable for the sensibility of red luminescence for the Eu(III) ions. The intensity ratio $I(^5D_0 \rightarrow ^7F_2)/I(^5D_0 \rightarrow ^7F_1)$ of ca. 1.6 indicates that the Eu(III) ions have a low symmetrical coordination environment. This is also consistent with the result of the single-crystal X-ray analysis. The room-temperature solid-state fluorescence lifetime of the sample was determined to be 232 μ s. This lifetime is shorter than that commonly observed for aromatic ligands in aqueous solutions suggesting one or more nonradiative pathways to assist in the deactivation of excited-state and thus the lifetime is shortened.¹⁵ It is known from X-ray structural data that ImDC³⁻ and ox²⁻ ligands does not encapsulate the entire metal as only two/three bidentate/tridentate ligands surround each metal leaving two sites ligated with water. Earlier work has established that a weak vibronic coupling between lanthanides and OH oscillators of coordinated water molecules provides a facile path for radiationless deexcitation of the metal ion.¹⁵ Thus, the lifetimes observed are expected to be shorter due to the direct coordination of water on the lanthanide.

The Dy-Zn-ImDC complex 6 was excited at 365 nm in the solid state at room temperature and gave a typical Dy³⁺ emission spectrum (Figure S6c, Supporting Information). The emission at 479, 577, and 658 nm is attributed to the characteristic emission of $^4F_{9/2} \rightarrow ^6H_J$ ($J = 15/2, 13/2$ and $11/2$) transitions of the Dy³⁺ ion. The relative intensity ratio for the emission lines at 479 and 573 nm is indicative of the larger probability for the $^4F_{9/2} \rightarrow ^6H_{15/2}$ transition. Compared with 3 (Sm³⁺) and 4 (Eu³⁺), the lifetime of complex 6 (Dy³⁺) is only about 3.3 μ s, which are comparable to other corresponding Dy(III)-based d-f heterometallic complex.¹⁶

To further explore the adsorption properties of the framework complexes on nitrogen and hydrogen. The dehydrated 3 and 6 are thermally stable up to 345 °C, shown in their TGA studies (Figures S1 and S10, Supporting Information), and they still keep crystalline forms; however, only powder crystal was obtained and then the X-ray crystal structures of dehydrated 3 and 6 were characterized (Figure S7, Supporting Information). Derived from the N2 sorption data, the BET surface areas are 639 m²/g (Langmuir surface area, 802 m²/g) for 3 and 526 m²/g (Langmuir surface area, 567 m²/g) for 6. PLATON¹⁷ calculations showed that the solvent-accessible volume constitutes

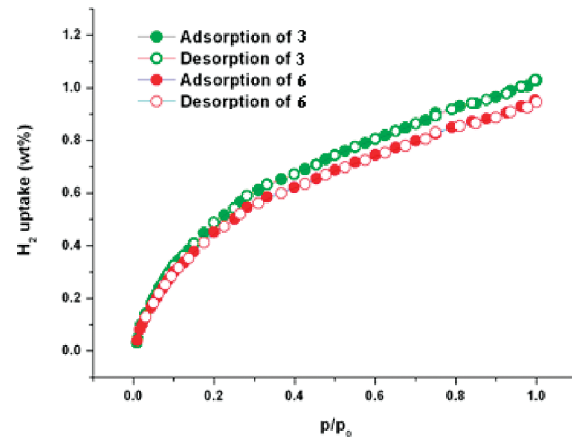


Figure 7. Isotherms of adsorption and desorption of hydrogen for 3 (green) and 6 (red) at 77 K.

about 21% of the total volume of the crystal 3 after being activated. Measured nitrogen adsorption of 3 at 77 K, shown in Figure 6, displays the typical type I sorption behavior and a dinitrogen uptake of approximately 105 cm³(STP)/g at $P/P_0 = 1.0$. With the same method, compound 6 only adsorbs 65 cm³/g of nitrogen at 77 K and 1 atm, though theory calculation showed that the solvent-accessible volume constitutes about 19% of the total volume of the crystal 6 which is very close to that of 3. This result can be attributed to the different shapes of 1-D channels in 3-D MOFs, namely, 1-D square channels with 7.3×6.0 Å for 3 and 1-D flat channels with 7.9×4.5 Å for 6 (Figures 3, 5, and S10). From Figure 7, the H₂ sorption isotherm at 77 K shows that the two compounds 3 and 6 have similar behaviors with an uptake of 1.10 wt % at 1 atm for 3 and 0.95 wt % for 6, which contributes to the pore volume of 6 being very close to that of 3 for small molecule H₂.

CONCLUSION

In summary, a family of 3-D lanthanide-zinc coordination frameworks with two structural types I and II are successfully constructed from mixed organic dicarboxylate ligand of 4, 5-imidazoledicarboxylate and oxalate under similar conditions. X-ray crystallography reveals that I structures including 1–4 involve the assembly of 2-D $[Zn_2(ImDC)_2]$ layers and 1-D $Ln_2(\mu_2-O)_2(ox)$ sine wave-like chains, while II structures including 4'–10 involve the assembly of 2-D $[Zn(ImDC)]_2$ layers and $[Ln_2(ox)]$ pillars, in which the change of the coordination numbers of lanthanide ion from 9 (for I) to 8 (for II) may be attributed to the lanthanide contraction effect. At the same time, among complexes 1–10, the average Ln–O bond lengths decrease with the increasing atomic number of the lanthanides, reflecting the effect of lanthanide contraction in Zn-4f system. Moreover, two types of europium complexes 4 and 4' can reversibly transform into each other, indicating the europium ion as a critical point in the structural variation from I to II in the present case. On the other hand, the adsorption and desorption behaviors of 3 and 6 on N₂ and H₂ also illustrate the impact of two different types of MOFs (I and II) on the properties of gas sorption. Meanwhile, the complexes 3, 4, and 6 exhibit characteristic lanthanide-centered luminescence. Obviously, the systematic investigation of a series of Ln-Zn-ImDC frameworks

should provide a rational synthetic strategy for constructing new photoluminescent and porous materials.

■ ASSOCIATED CONTENT

Supporting Information. Additional structural figures for the related compounds, and the TG curves of compound **2** and **6**, the luminescent spectra of compounds **3**, **4**, and **6** as well as X-ray crystallographic files in CIF format for compounds **1–4'**, and **5–10**. This material is available free of charge via the Internet at <http://pubs.acs.org>.

■ AUTHOR INFORMATION

Corresponding Author

*Phone: +86-20-39310383. Fax: +86-20-39310187. E-mail: ypcai8@yahoo.com.

■ ACKNOWLEDGMENT

The authors are grateful for financial aid from the National Natural Science Foundation of P. R. China (Grant Nos. 20772037 and 21071056), Science and Technology Planning Project of Guangdong Province (Grant Nos. 2006A10902002 and 2010B031100018), and the N. S. F. of Guangdong Province (Grant Nos. 9251063101000006 and 10351063101000001).

■ REFERENCES

- (1) (a) Lee, J. Y.; Farha, O. K.; Roberts, J.; Scheidt, K. A.; Nguyen, S. B. T.; Hupp, J. T. *Chem. Soc. Rev.* **2009**, *38*, 1450. (b) Lombardi, J. R.; Davis, B. *Chem. Rev.* **2002**, *102*, 2431. (c) Rinck, J.; Novitchi, G.; Van den Heuvel, W.; Ungur, L.; Lan, Y.; Wernsdorfer, W.; Anson, C. E.; Chibotaru, L. F.; Powell, A. K. *Angew. Chem., Int. Ed.* **2010**, *49*, 7583. (d) Chilton, N. F.; Langley, S. K.; Moubaraki, B.; Murray, K. S. *Chem. Commun.* **2010**, *46*, 7787. (e) Colacio, E.; Palacios, M. A.; Rodriguez-Dieguez, A.; Mota, A. J.; Herrera, J. M.; Choquesillo-Lazarte, D.; Clerac, R. *Inorg. Chem.* **2010**, *49*, 1826. (f) Karotsis, G.; Evangelisti, M.; Dalgarno, S. J.; Brechin, E. K. *Angew. Chem., Int. Ed.* **2009**, *48*, 9928. (g) Bo, Q.-B.; Sun, G.-X.; Geng, D.-L. *Inorg. Chem.* **2010**, *49*, 561. (h) Xiang, S.-C.; Hu, S.-M.; Sheng, T.-L.; Chen, J.-S.; Wu, X.-T. *Chem.—Eur. J.* **2009**, *15*, 12496. (i) Chen, W.-X.; Ren, Y.-P.; Long, L.-S.; Huang, R.-B.; Zheng, L.-S. *CrystEngComm* **2009**, *11*, 1522.
- (2) (a) Kong, X.-J.; Ren, Y.-P.; Chen, W.-X.; Long, L.-S.; Zheng, Z.; Huang, R.-B.; Zheng, L.-S. *Angew. Chem., Int. Ed.* **2008**, *47*, 2398. (b) Xiang, S.-C.; Hu, S.-M.; Sheng, T.-L.; Fu, R.-B.; Wu, X.-T.; Zhang, X.-D. *J. Am. Chem. Soc.* **2007**, *129*, 15144. (c) Chen, X.-M.; Aubin, S. M. J.; Wu, Y.-L.; Yang, Y.-S.; Mak, T. C. W.; Hendrickson, D. N. *J. Am. Chem. Soc.* **1995**, *117*, 9600. (d) Cai, Y.-P.; Li, G.-B.; Zhan, Q.-G.; Sun, F.; Xu, A.-W. *J. Solid State Chem.* **2005**, *178*, 3729. (e) Cai, Y.-P.; Su, C.-Y.; Li, G.-B.; Mao, Z.-W.; Zhang, C.; Xu, A.-W.; Kang, B.-S. *Inorg. Chim. Acta* **2005**, *358*, 1298. (f) Cai, Y.-P.; Yu, Q.-Y.; Zhou, Z.-Y.; Hu, Z.-J.; Fang, H.-C.; Wang, N.; Zhan, Q.-G.; Chen, L.; Su, C.-Y. *CrystEngComm* **2009**, *11*, 1006. (g) Cai, Y.-P.; Zhou, X.-X.; Zhou, Z.-Y.; Zhu, S.-Z.; Thallapally, P. K.; Liu, J. *Inorg. Chem.* **2009**, *48*, 6341.
- (3) (a) Cotton, F. A.; Wilkinson, G.; Murrillo, C. A.; Bochmann, M. *Advanced Inorganic Chemistry*, 6th ed.; Wiley: New York, 1999; p 1108. (b) Mizukami, S.; Houjou, H.; Kaneko, M.; Hiratani, K. *Chem.—Eur. J.* **2003**, *9*, 1521. (c) Liu, M.-S.; Yu, Q.-Y.; Cai, Y.-P.; Su, C.-Y.; Lin, X.-M.; Zhou, X.-X.; Cai, J.-W. *Cryst. Growth Des.* **2008**, *8*, 4083. (d) Roos, B. O.; Pykkö, P. *Chem.—Eur. J.* **2010**, *16*, 270. (e) Wang, H.-Y.; Cheng, J.-Y.; Ma, J.-P.; Dong, Y.-B.; Huang, R.-Q. *Inorg. Chem.* **2010**, *49*, 2416. (f) Seitz, M.; Oliver, A. G.; Raymond, K. N. *J. Am. Chem. Soc.* **2007**, *129*, 11153. (g) Parker, D.; Puschmann, H.; Batsanov, A. S.; Senanayake, K. *Inorg. Chem.* **2003**, *42*, 8646.
- (4) (a) Cheng, J.-W.; Zhang, J.; Zheng, S.-T.; Zhang, M.-B.; Yang, G.-Y. *Angew. Chem. Int. Ed.* **2006**, *45*, 73. (b) Aronica, C.; Pilet, G.; Chastanet, G.; Wernsdorfer, W.; Jacquot, J.-F.; Luneau, D. *Angew. Chem., Int. Ed.* **2006**, *45*, 4659.
- (5) (a) Sun, Y.-Q.; Zhang, J.; Yang, G.-Y. *Chem. Commun.* **2006**, 1947. (b) Zou, R.-Q.; Sakurai, H.; Xu, Q. *Angew. Chem., Int. Ed.* **2006**, *45*, 2542. (c) Gao, G.-G.; Xu, L.; Wang, W.-J.; Qu, Xiao-S.; Liu, H.; Yang, Y.-Y. *2008*, *47*, 2325. (d) Xu, Q.; Zou, R.-Q.; Zhong, R.-Q.; Kachi-Terajima, C.; Takamizawa, S. *Cryst. Growth Des.* **2008**, *8*, 2458. (e) Gurunatha, K. L.; Uemura, K.; Maji, T. K. *Inorg. Chem.* **2008**, *47*, 6578. (f) Alkordi, M. H.; Liu, Yunling, L.; Randy, W.; Eubank, J. F.; Eddaoudi, M. *J. Am. Chem. Soc.* **2008**, *130*, 12639. (g) Wang, S.; Zhang, L.-R.; Li, G.-H.; Huo, Q.-S.; Liu, Y.-L. *CrystEngComm* **2008**, *10*, 1662. (h) Liu, Y.-L.; Kravtsov, V. Ch.; Eddaoudi, M. *Angew. Chem., Int. Ed.* **2008**, *47*, 8446. (i) Alkordi, M. H.; Brant, Jaclyn, A.; Wojtas, L.; Kravtsov, V. Ch.; Cairns, A. J.; Eddaoudi, M. *J. Am. Chem. Soc.* **2009**, *131*, 17753. (j) Feng, X.; Wang, L.-Y.; Zhao, J.-S.; Wang, J.-G.; Ng, S. W.; Liu, B.; Shi, X.-G. *CrystEngComm* **2010**, *12*, 774. (k) Feng, X.; Liu, B.; Wang, L.-Y.; Zhao, J.-S.; Wang, J.-G.; Ng, W. S.; Shi, X.-G. *Dalton Trans.* **2010**, *39*, 8038.
- (6) (a) Sun, Y.-Q.; Zhang, J.; Yang, G.-Y. *Chem. Commun.* **2006**, 4700. (b) Li, Z.-Y.; Dai, J.-W.; Qiu, H.-H.; Yue, S.-T.; Liu, Y.-L. *Inorg. Chem. Commun.* **2010**, *13*, 452. (c) Zhang, Q.; Zheng, Y.-X.; Liu, C.-X.; Sun, Y.-G.; Gao, E.-J. *Inorg. Chem. Commun.* **2009**, *12*, 523. (d) Sun, Y.-G.; Yan, X.-M.; Ding, F.; Gao, E.-J.; Zhang, W.-Z.; Verpoort, F. *Inorg. Chem. Commun.* **2008**, *11*, 1117.
- (7) (a) Gu, Z.-G.; Cai, Y.-P.; Fang, H.-C.; Zhou, Z.-Y.; Thallapally, P. K.; Tian, J.; Exarhos, G. *J. Chem. Commun.* **2010**, *46*, 5373. (b) Gu, Z.-G.; Wang, M.-F.; Peng, H.-M.; Li, G.-Z.; Yi, X.-Y.; Gong, X.; Fang, H.-C.; Zhou, Z.-Y.; Cai, Y.-P. *Inorg. Chem. Commun.* **2010**, *13*, 1439. (c) Gu, Z.-G.; Chen, J.-H.; Chen, Y.-N.; Ying, Y.; Peng, H.; Jia, H.-Y.; Wang, M.-F.; Li, S.-S.; Cai, Y.-P. *Inorg. Chem. Commun.* **2010**, *14*, 68.
- (8) Sheldrick, G. M. SADABS, Version 2.05; University of Göttingen: Göttingen, Germany.
- (9) Sheldrick, G. M. *SHELXS-97, Program for X-ray Crystal Structure Determination*; University of Göttingen: Göttingen, Germany, 1997.
- (10) Sheldrick, G. M. *SHELXS-97, Program for X-ray Crystal Structure Refinement*; University of Göttingen: Göttingen, Germany, 1997.
- (11) Nakamoto, K. *Infrared and Raman Spectra of Inorganic and Coordination Compounds*; John Wiley and Sons: New York, 1997.
- (12) (a) Zhou, X.-X.; Liu, M.-S.; Lin, X.-M.; Fang, H.-C.; Chen, J.-Q.; Yang, D.-Q.; Cai, Y.-P. *Inorg. Chim. Acta* **2009**, *362*, 1441. (b) Tao, J.; Yin, X.; Wei, Z.-B.; Huang, R.-B.; Zheng, L.-S. *Eur. J. Inorg. Chem.* **2004**, *125*. (c) Zhou, Q.-D.; Hambley, T. W.; Kennedy, B. J.; Lay, P. A.; Turner, P.; Warwick, B.; Biffin, J. R.; Regtop, H. L. *Inorg. Chem.* **2000**, *39*, 3742. (d) Lin, X.-M.; Fang, H.-C.; Zhou, Z.-Y.; Chen, L.; Zhao, J.-W.; Zhu, S.-Z.; Cai, Y.-P. *CrystEngComm* **2009**, *11*, 847.
- (13) Brito, H. F.; Malta, O. L.; Felinto, M. C. F. C.; Teotonio, E. E. S.; Menezes, J. F. S.; Silva, C. F. B.; Tomiyama, C. S.; Carvalho, C. A. A. *J. Alloys Comp.* **2002**, *344*, 293.
- (14) (a) Regulacio, M. D.; Pablico, M. H.; Vasquez, J. A.; Myers, P. N.; Gentry, S.; Prushan, M.; Tam-Chang, S.-W.; Stoll, S. L. *Inorg. Chem.* **2008**, *47*, 1512. (b) Hakala, H.; Liitti, P.; Puukka, K.; Peuralahti, J.; Loman, K.; Karvinen, J.; Ollikka, P.; Ylikoski, A.; Mukkala, V.; Hovinen, J. *Inorg. Chem. Commun.* **2002**, *5*, 1059.
- (15) Latva, M. *J. Lumin.* **1997**, *75*, 149.
- (16) Li, Z.-Y.; Dai, J.-W.; Wang, N.; Qiu, H.-H.; Yue, S.-T.; Liu, Y.-L. *Cryst. Growth Des.* **2010**, *10*, 2746.
- (17) Spek, A. L. *J. Appl. Crystallogr.* **2003**, *36*, 7.